ELECTRICAL CLASSIFICATION OF SINGLE RED BLOOD CELL DEFORMABILITY IN HIGH SHEAR MICRO-CHANNEL FLOWS

Y. Katsumoto, K. Tatsumi*, T. Doi, K. Nakabe
Kyoto University, Kyoto, Japan

ABSTRACT. Measurement of human red blood cell (RBC) deformability in a micro-channel using electric micro-sensors is proposed and carried out in this study. The time series of the electric resistance is measured using an alternative current vs. voltage (I-V) method as the RBCs deformed by high shear flows individually pass between the electrodes. The resistance distributions vary in relation with the RBC shape, which depends on the cell deformability under the condition of a constant shear stress produced by the flow. Experiment is carried out with the samples of normal and glutaraldehyde treated (rigidized) RBC to evaluate the feasibility of the present method.

Keywords: *Micro-channel, Red blood cell, Deformability, Micro electric resistance sensor*

INTRODUCTION

Measurement of the deformability of a red blood cell (RBC) is an important issue in terms of not only investigating the hydrodynamic characteristics of the blood such as fluid viscosity and electric permeability[1], but also diagnosing initial symptoms of diseases in clinical investigation. For example, in *Plasmodium falciparum*, which is one of the most virulent diseases causing severe anaemia in number of tissues and organs[2], the deformability of the RBC is significantly reduced due to the increase of the internal viscosity and rigidization of the cytomembrane caused by having the plasmcytoskeleton of the RBC bounded with the neoantigens during the parasite, even in the early 'ring' stage[3]. Therefore, developing a technique which can evaluate the deformability of the RBC with low cost, short time and simplified procedure would provide a large contribution in the medical fields particularly in clinical testing[3,4].

There are several typical measuring schemes to evaluate the RBC deformability. The one using viscometer[5] evaluates the deformability of the bulk RBC solutions from the fluid viscosity. The one using a rheometer with coaxial rotating cylinder applies shear stress on the RBC and measures the deformability visually[6]. Measurement using optical tweezers[7] or micro-glass pipettes[8] stretches single RBC and evaluates the extension rate. However, the accuracy of the former two measuring schemes is low especially when the number density of infected RBC is small. This is not preferable for clinical test of diseases in the early stages. On the other hand, the latter two can evaluate the deformability of each single RBC whereas the available sampling number of RBC is limited.

The motivation of the present study is to develop a micro sensor which can measure the deformability of a single RBC using hydrodynamic stresses and electrical sensors applied in a micro-channel. Recently, Korin et al.[9] visualized the behaviour of RBCs in a micro-channel and measured the cell deformation by analysing the images of the cells stretched by the high shear flow. The usage of the micro-channel has the advantage in reducing the cost, measuring time, and sample volumes. Their method, however, requires high spatial resolution image recording equipment, which may increase the cost and impair the compactness of the application. In contrast, the sensor proposed in the present study is based on an electrical measurement to evaluate the RBC deformation. Namely, micro platinum membrane electrodes are attached to the channel bottom wall

* Corresponding author: Dr. K. Tatsumi
Phone: + (81)-75-7535209, Fax: + (81)-75-7535209
E-mail address: tatsumi@mbox.kudpc.kyoto-u.ac.jp

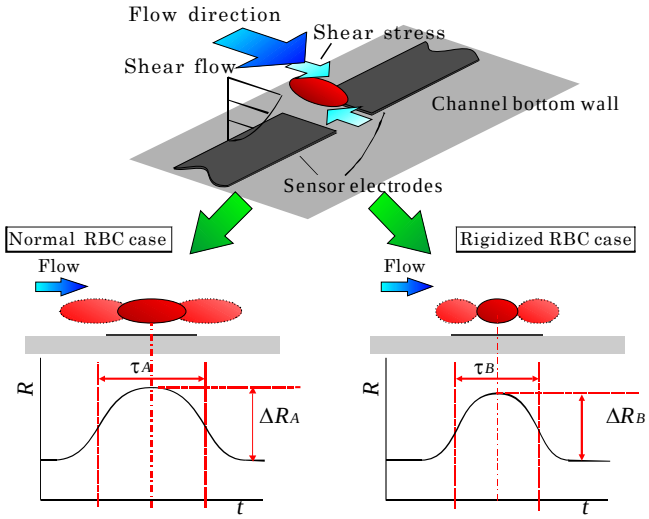

Figure 1. Concept of the measuring method of RBC deformability.

of the sensor, and the time-sequential signals of electric resistance are measured as the RBC crosses the electrodes. Compared with the aforementioned optical measurements, the present method can decrease the size and cost of the device markedly. A higher affinity to the existing RBC counting equipments is also another advantage. In this paper, experiment is carried out to evaluate the feasibility of the sensor proposed in this study. Micro-channel with the micro membrane electrodes is fabricated, and the electric resistances of the RBC crossing the electrodes are measured and analysed using the samples of normal human RBC and glutaraldehyde-treated rigidized RBC.

MEASUREMENT PHYSICS

The electric conductivity of the RBC cytomembrane is approximately 1×10^{-6}S/m, which is small enough to be considered as an insulating material compared with the cytoplasm and normal saline solution. When a low frequency AC electric field is applied around the RBC suspended in a solution, the current is interfered mainly by the cytomembrane. In this case, the cell shape also affects the distribution of the current density, in other words, the electric resistance monitored between the electrodes changes depending on the cell shape.

Figure 1 shows the schematic of the measuring method proposed in this study. A pair of platinum membrane electrodes is attached to the bottom wall of a micro-channel, and the time-sequential signals of the electric resistance between the electrodes are measured. When RBCs are suspended in the micro-channel flow, the resistance between the electrodes increases significantly as the RBC passes between them due to its high electric insulating property. While the RBCs flow in the channel, they are stretched and deformed attributed to the high shear stress provided by the steep velocity gradient of the flow. The profile of the measured resistance is affected not only by the fluid properties but also by the size, position and shape of the RBC. If the position of the RBC passing between the electrodes can be precisely controlled, then the shape of the RBC, which also represents the deformability of the RBC, can be evaluated by analysing the resistance signals.

When an electric field is, thus, applied to the RBC by using the sensor shown in Fig. 1, the parallel circuit between the electrodes consists of cytoplasm, cytomembrane, solvent, and the electric double layer formed at the electrode surface as shown in Fig. 2(a). This circuit can also be simplified as parallel components of variable resistance and capacitance connected in series with the component of the electric double layer, presenting the change in the electric characteristics as the RBC passes between the electrodes.

As one can see, the accuracy of the measurement largely relies on how large the difference between the resistances of the buffer solution and the RBC membrane is. If a solution of high ionic concentration, such as isotonic sodium chloride solution, is used, however, the effect of the electric double layer cannot be neglected. This problem can be solved by applying a high frequency AC electric field to the electrodes and reducing the capacitance of the electric double layer. In contrast,

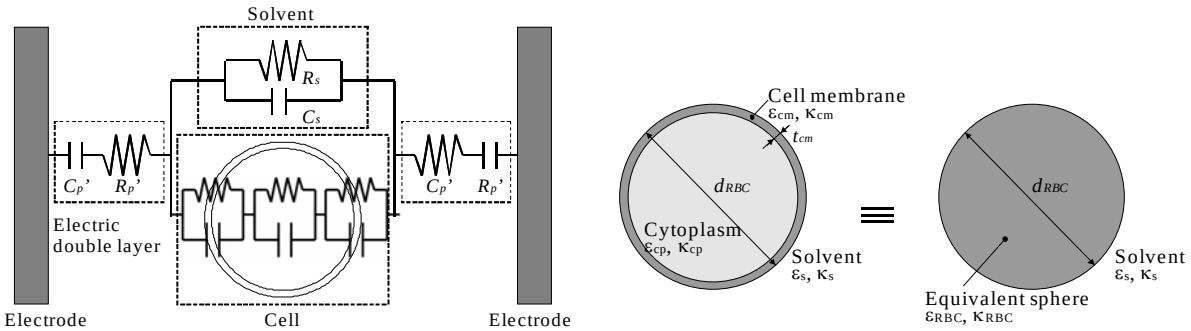

(a) Equivalent circuit (b) Cell model

Figure 2. (a) Equivalent circuit model of the sensor with an RBC suspended in a solvent, (b) Cell model simplified as a sphere in the numerical simulation.

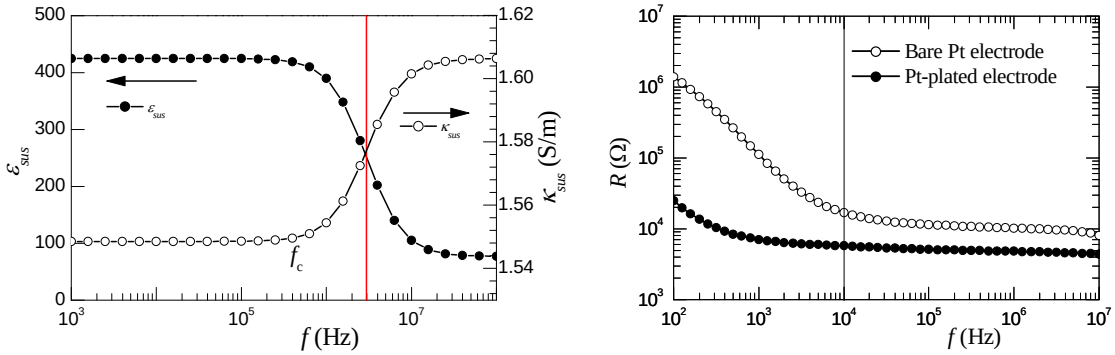

(a) Effects of f on ε and κ (sim.) (b) Effects of f on R (exp.)

Figure 3. AC frequency effects on (a) permittivity ε and conductivity κ of RBCs suspended in PBS (simulation), and (b) the resistance of the PBS without RBC (experiment).

since the cell membrane has electrically insulation properties, an increase in the frequency of the electric field can incur a decrease of the cell resistance. Therefore, there is a trade-off problem in determining the frequency range to be applied on the electrodes.

The maximum limit of the frequency is obtained from the numerical simulation calculating the impedance characteristic of RBCs suspended in the solution using the model proposed by Katsumoto et al.[10]. This model treats the RBC as a 6μm diameter sphere shown in Fig. 2(b) having the frequency-dependent complex permittivity derived form from the Maxwell-Wagner equation.

Figure 3(a) depicts the results of the computation showing the effects of the frequency, f, on ε and κ, respectively. κ increases with f in the area above several MHz in the figure showing the relaxation behaviour of the solution. This indicates that the cytomembrane acts as an insulator when the frequency is low, while the cytoplasm is directly measured when the frequency is high. As mentioned above, the present sensor shows a higher performance with larger difference in the solution and RBC. Therefore frequency of several tens of kHz is suitable for the sensors. The lower limit of the frequency to be applied will be discussed shortly.

EXPERIMENTAL SETUP

Figure 4 and Table 1 show the schematic and dimensions of the channel and sensor electrodes used in this study, respectively. The channel width is 1mm and is much larger than the channel heights H_1 and H_2. Therefore, the channel flow can be considered as two-dimensional flow, and the RBC is deformed receiving the shear stress in the streamwise direction.

The channel has three inlets, and RBCs suspended in phosphate buffer saline (PBS: Amresco) solution are supplied from the center inlet while PBS solution only is supplied from the side ones. Due to the low Reynolds number of the flow in the micro-channel, the flow is in laminar regime and the molecular diffusion of the flow supplied from the center inlet becomes small. Therefore, by

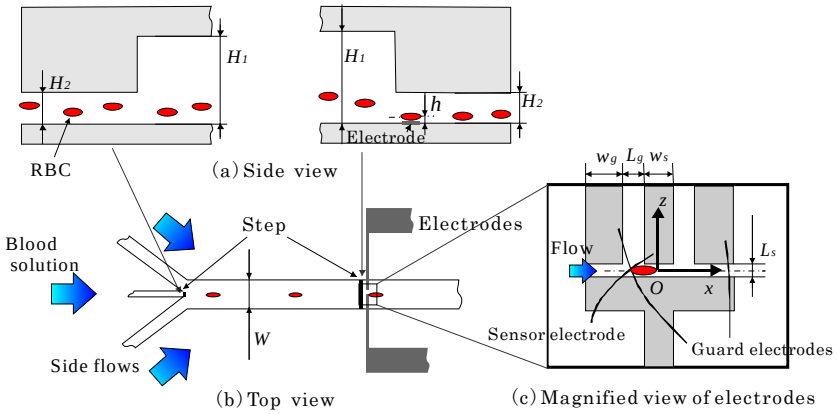

Figure 4. Schematic of the micro-channel and sensor electrodes.

Table 1. Parameters of the micro-channel and electrodes (μm).

W	H_1	H_2	L_s	L_g	w_s	w_g
1000	52	10	5.2	2.3	14.8	14.6

changing the flow rate of each side flow, the spanwise position of the RBC passage can be controlled to pass the center of the electrodes. These fluids are supplied by syringe pumps (Nihon Kohden: CFV-3200, Harvard Apparatus: econoflo) with flow rates of 0.01 and 1.0μl/min.

When the RBC is placed in the channel shear flow, the RBC receives a lift force attributed to the so-called Fåhraeus effect[11]. This lift force moves the RBC away from the channel wall on which the sensor electrodes are embedded. Apparently, this leads to a decrease of the measuring resistance and the sensor S/N ratio. To tackle this problem, the channel heights at the center inlet and at the electrodes are smaller than the other parts of the channel, i.e. backward-facing and forward-facing steps are installed in the downstream of the center inlet and immediately upstream of the electrodes, respectively. The RBC is, thus, supplied from the inlet in a lower position, and the downwash flow at the forward-facing step carries the RBC toward the bottom wall. This spanwise and downward positioning of the RBC passage can control the relative distance between the RBC and electrodes.

The micro-channel illustrated in Fig. 4 is made of poly-dimethylsiloxane (PDMS) and is fabricated by using SU-8 (MicroChem) as a casting mold. To fabricate the SU-8 mold, an optical mask, on which the channel pattern is printed, is prepared first. Then, SU-8 layer spincoated on a slide glass is exposed to the UV light through the mask. After the post baking and etching processes, an SU-8 mold is obtained. PDMS in liquid phase is then poured over the SU-8 mold, and is rigidized and ripped off. The PDMS channel is then attached to a slide glass, on which the platinum membrane patterns of electrodes are formed. These electrodes are fabricated through a sputtering and lift-off processes using a sputtering equipment (ULVAC KIKO: SCOTT-C3) and ZPN (ZEON) resist.

The electrodes are serially connected to the shunt resistance for detection. Sinusoidal wave of AC voltage is applied to these resistances under the condition of 10kHz using a function generator (NF: WF-1973). By measuring the phases of the shunt resistance and applied voltages, the resistance measurement accuracy is enhanced.

As shown in Fig. 4, guard electrodes are placed on both sides of the sensor electrode (the one used for detection). Voltage is charged to these guard electrodes through an FET input Op-amp possessing the same electric potential with the sensor electrode. The electric fluxes from the guard electrodes will suppress the fringe effect of the fluxes from the sensor electrode. This leads to a narrow distribution of the current density in the streamwise direction and enhances the sensitivity.

To evaluate the impedance characteristic of the electrodes, the electric resistance between the electrodes embedded in the channel filled with PBS solution is first measured by using an impedance analyser (Agilent: 4294A). Figure 3(b) shows how the frequency of the applied AC voltage, f , affects the resistance, R. The open and solid circles in the figure present the results using platinum bare electrodes and platinum black plated ones, respectively. The Pt-plated electrodes represent those with Pt nano particles attached on the surface using the following plating process.

Namely, first filling the channel with a solution of hexachloroplatinic (H_2PtCl_6) 30mg/mL and lead acetate $(CH_3COO)_2Pb$ 0.3mg/mL, and then applying 2V DC voltage between the electrodes.

As shown in Fig. 2(a), when *f* is not sufficiently high, an electrical double layer is formed at the electrode surfaces, which leads to a reduction in the resistance measurement performance. This can be observed in Fig. 3(b), where the resistance *R* plotted with the open circles decreases as *f* increases and then becomes constant. As mentioned above, 10kHz AC electric field is applied in this study. This is, however, not large enough to suppress the appearance of the electric double layer as can be found in Fig. 3(b), i.e. *R* measured under the condition of *f* = 10kHz is larger than the values in higher frequency region. To tackle this problem, the aforementioned Pt-black plating is conducted on the electrode surface in this study. A layer of Pt nano-particles will be formed on the surface as a porous media, and the surface area is increased by this structure resulting in the reduction of the electric double layer effect. In this case, the frequency range from which *R* begins to increase is shifted toward the lower *f* side and *R* is small and uniform under the condition of *f* = 10kHz compared with the case of bared electrodes. It should be noted that the reason why the resistance in the plated case are lower than those of the bare electrodes is attributed to the fact that the plate is formed uniformly on the surface and the distance between the electrodes is decreased.

Along with the above electric measurements, optical measurement is carried out using a microscope (Olympus: IX-71) and halogen lamp as the light source for the purpose of verifying the position and shape of the RBC when passing between the electrodes. An objective lens (Olympus: LMPLFLN100X, ×100 magnification and *NA* = 0.8) and a high speed camera (Vision Research: Phantom V7.3) are used to record the images. The frame rate of the camera is 1000 frames/s and the CCD resolution is 800×650 pixels. The optical resolution of the image is 0.21μm/pixel. The focusing depth of the image Δz is 1.669μm calculated from the following equation:

$$\Delta z = \frac{\lambda_0 n}{NA^2} + \frac{n}{MNA} e \qquad (1)$$

e and *M* are the smallest distance that can be resolved by the detector, and lateral magnification, respectively. λ_0 and *n* are the wave length of light in air and refraction index.

Korin et al. [13] reported that shear stress required to deform an RBC with a deformation index *DI*=0.5 in a micro-channel is approximately 15Pa. Here, *DI* is defined as $DI = (a-b)/(a+b)$, where *a* and *b* are the long and short axes of the RBC, respectively. When water is used as the working fluid, it is not suitable to obtain this value of shear stress by increasing the flow rate because of the time resolution of the measurement using the high-speed camera and electric sensors. Polyvinylpyrrolidone (PVP: MW 3.6×10^5, Nacalai tesque) is, therefore, mixed with the working fluid to increase the viscosity, by which sufficient shear stress is achieved to deform the RBC.

RBC treatment is carried out by the following procedure. 10μl sample blood is collected from a healthy human volunteer. The blood is first suspended in 1ml PBS, and then centrifuged during 10min with 1000G to separate the RBC from other substances, i.e. plasma, plaque and leucocytes. Supernatant solution is removed, and 0.1ml PBS is added to the collected RBC. 0.4ml PBS with 10wt% PVP is added to the solution, and RBC suspended solution of PBS with 8wt% PVP is prepared and used as the normal RBC suspended working fluid.

Rigidized RBCs are prepared by treating the cells with glutaraldehyde. Glutaraldehyde (Nakalai tesque: 25% solution) is first diluted with PBS by 0.025wt%. The RBC separated from other substances in the same way shown above is then added to this solution and settled for 30min under room temperature. The solution is, then, centrifuged during 10min with 1000G. After removing the supernatant solution, 1ml PBS is added. Once again the solution is centrifuged and the supernatant solution is removed. Finally, 0.1ml PBS and 0.4ml PBS with 10wt% PVP are respectively added to the solution, and, thus, PBS solution of 8wt% PVP with rigidized RBC is prepared.

EXPERIMENTAL RESULTS

Figures 5(a) and (b) show the snapshots presenting the behaviour of the normal and rigidized RBCs passing between the electrodes, respectively. The flow direction is from the left to the right, and the

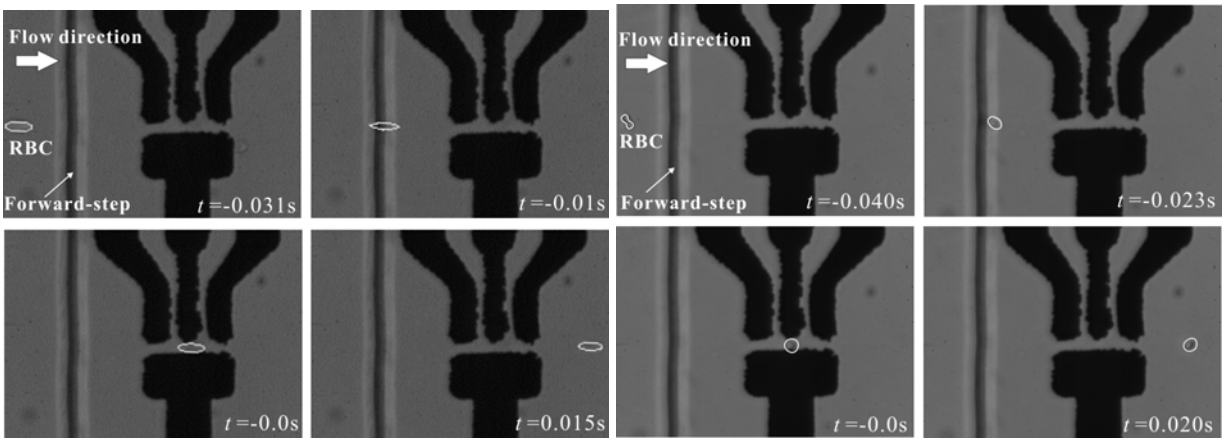

(a) Normal RBC case (b) Rigidized RBC case

Figure 5. Snapshots of RBCs passing between the electrodes.

Table 2. Averaged value of the major and minor axes of the RBC and deformation index, *DI*.

	Normal RBC	Rigidized RBC
a [μm]	14.54	7.37
b [μm]	4.65	7.35
DI	0.52	0.00

arrow indicates the location of the forward-facing step. Although not shown here, the height of the RBC passage, *h*, was obtained visually by measuring the distance between the points focused on the RBC and bottom wall. *h* was nearly constant for all RBC measured as h=5μm. It should be noted that the degree of the error in *h* is approximately equal to the aforementioned focusing depth Δz.

In the figure, the RBC is deformed and stretched in the streamwise direction owing to the two-dimensional shear flow in the channel. In Fig. 5(a), the RBC deforms most when passing the forward-step. This is due to downward flow generated at the step by which not only the shear stress is increased, but also the RBC is carried to the area of larger shear stress located close to the bottom wall. The deformation rate gradually decreases as the RBC flows to the downstream. This can be attributed to the Fåhraeus effect[11], namely, a lift force works on the RBC and the RBC moves toward the channel center resulting in a reduction of the shear stress.

In contrast with the normal RBC case, the rigidized RBC shown in Fig. 5(b) maintains a biconcave surface and no deformation of the cell is observed. The RBC rotates as it flows, which is a motion so called 'flipping'. When a normal RBC is suspended in a shear flow, the cytomembrane not only deforms but also rotates together with the cytoplasm. This is called 'tank treading motion' of the cell, which prevents the cell to flip[12]. Since the shape of the cytomembrane in the rigidized RBC case is fixed, the tank treading motion cannot be generated and the flipping motion takes place.

Table 2 shows the averaged value of the long and short axes of the RBC, *a* and *b*, and the deformation index, *DI* , obtained from the visualization results. As mentioned above, rigidized RBCs show no deformation and have a circle projection shape. Therefore *a* and *b* are identical in this case. On the other hand, since the normal RBC is deformed, *a* is almost three times larger than *b*. *DI* is approximately 0.5 in the normal RBC case.

Figure 6 shows the distributions of ΔR_{max} and δ of the normal and rigidized RBCs. ΔR_{max} and δ are the maximum value and half bandwidth of the resistance peak distributions obtained when each RBC passes the electrodes, respectively. During the experiment, variation in the RBC spanwise position when passing the electrodes is observed. This is attributed to the width of the center inlet of the channel, which is 50μm and is much larger than the gap between the electrodes, L_g =5μm . To discuss this effect, the spanwise position of the cell, y_{RBC}, is taken as the abscissa in the figure. The lines in the figure present the results obtained by using the least-square method (L.S.M.) in each RBC case.

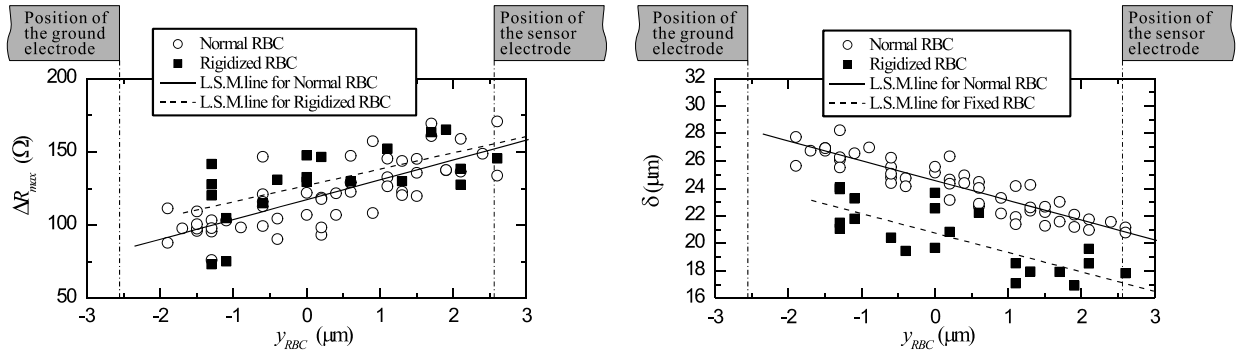

(a) Relation between ΔR_{max} and y_{RBC} (b) Relation between δ and y_{RBC}

Figure 6. Distributions of peak resistance ΔR_{max} and half bandwidth δ against spanwise location of RBC, y_{RBC}.

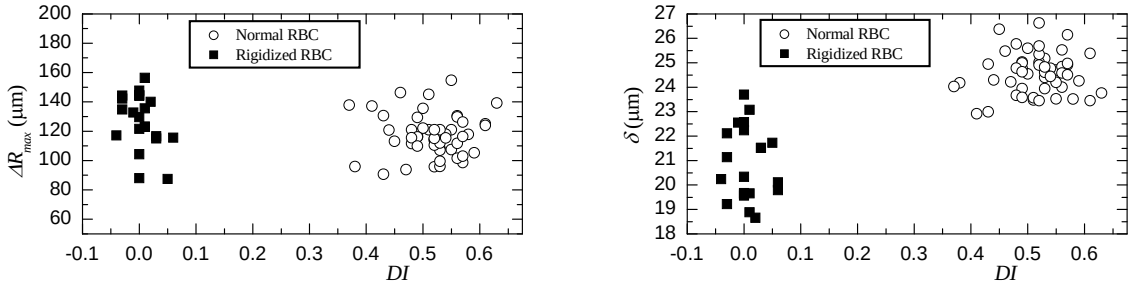

(a) Relation between ΔR_{max} and *DI* (b) Relation between δ and *DI*

Figure 7. Distributions of modified ΔR_{max} and δ against deformation index *DI*.

In Fig. 6 (a), ΔR_{max} decreases as the RBC position y_{RBC} is closer to the ground electrode. On the other hand, δ increases as y_{RBC} decreases as shown in Fig. 6(b). This can be attributed to the following reason: As seen in Figs. 4 and 5, the sensor side consists of three electrodes, the sensor and guard electrodes, while the ground side has a single electrode. The effect of the guard electrodes reducing the fringe components of the electric flux deteriorates in the ground side. Namely, the current density distribution becomes wide and the value decreases in the position close to the ground electrode. The amount of electric flux blocked by the RBC, therefore, decreases, which leads to a decrease in the resistance particularly the maximum value, ΔR_{max}. On the other hand, since the current density distribution is wider at the location close to the ground electrode, δ increases.

As shown in Fig. 6, y_{RBC} appears to affect ΔR_{max} and δ linearly. Therefore, the linear component using the L.S.M. line in the figure is subtracted from each value, and is shown in Fig. 7 in relation with *DI*. Since only two kinds of RBCs, normal and glutaraldehyde-treated ones, are measured in the experiment, two large groups are found in the area close to *DI* = 0.0 and 0.5.

To evaluate the variation of the samples in each RBC case, coefficient of variance, $Cv=\sigma/m\times100$, is shown in Table 3. σ and m are the standard deviation and arithmetic average of the distributions, respectively.

In Fig. 7(a), ΔR_{max} of both RBCs show similar values and overlap with each other. Furthermore, *Cv* of ΔR_{max} shown in Table 3 is relatively large in both RBC cases, indicating that the variation of the samples is large.

On the other hand, a difference in the groups of δ for the normal and rigidized RBCs is recognizable in Fig. 7(b) indicating the fact that there is a correlation between δ and *DI*. Furthermore, *Cv* shown in Table 3 is small compared with those of ΔR_{max} . These results point out that the half bandwidth δ is more reasonable as an index to evaluate the shape, i.e. deformability of the RBC, than ΔR_{max}.

The reason why δ shows a better characteristic than ΔR_{max} is due to current density distribution between the electrodes. ΔR can be more sensitive with the RBC height position *h*. Therefore, even when the RBC height position is controlled by the step flow, small variation in *h* can vary ΔR_{max}

Table 3. Coefficient of variance for ΔR_{max} and δ

	ΔR_{max}		δ	
	Normal RBC	Rigidized RBC	Normal RBC	Rigidized RBC
Cv (%)	12.1	15.4	3.42	7.39

largely enough to make the difference of the RBC shape ambiguous. δ, however, depends more on the current density distribution in the streamwise direction, which is less affected by other parameters.

CONCLUSIONS

A micro sensor consisted of micro-channel and electric sensors, which can measure the deformability of a single RBC was proposed and evaluated in this study. The sensor was fabricated and its feasibility was examined using normal and rigidized human red blood cells. The major results are stated as follows:

1. The frequency of the sensor AC voltage was determined numerically and experimentally. Together with the Pt-black plated on the electrodes, frequency specification of 10kHz reduced the influences of the electric double layer formed on the electrodes and dielectric relaxation appearing around the cell membrane, which led to the increase of the sensor sensitivity.
2. The backward- and forward facing steps, and the side flows applied in the micro-channel were effective to control the height and spanwise positions of the RBC in order to closely pass the area between the sensor electrodes.
3. A good correlation was observed between the half bandwidth of the time-sequential signals of the resistance and the deformation index. In contrast, the correlation between the peak value of the resistance and deformation index was considerably small. This characteristic was strongly attributed to the current density distribution formed between the electrodes. Consequently, the feasibility of the present sensor was verified from the results.

ACKNOWLEDGEMENT

This study was financially supported by The Japanese Ministry of Education, Culture, Sports, Science.

REFERENCES

1. Sugihara-Seki, M. and Fu, B. M., Blood Flow and Permeability in Microvessels, *Fluid Dynamics Research*, Vol. 37, pp. 82-132, 2005.
2. Miller, L. H., Baruch, D. I., Marsh, K. and Doumbo, O. K., The Pathogenic Basis of Malaria, *Nature*, Vol. 415, pp. 673-679, 2002.
3. Dondorp, A. M., Kager, P. A., Vreeken, J. and White, N. J., Abnormal Blood Flow and Red Blood Cell Deformability in Severe Malaria, Parasitology Today, Vol. 16, pp. 228-232, 2000.
4. Lim, C. T., Zhou, E. H. and Quek, S. T., Mechanical Models for Living Cells – a Review, *J. Biomechanics*, Vol. 39, pp. 195-216, 2006.
5. Chien, S., Biophysical behavior of Red Cells in Suspension, *In the Red Blood Cell* (*Ed. Surgenor, D. M.*), Vol. 2 (1975), Academic Press, New York, pp. 1031-1133, 1975.
6. Dobbe, J. G. G., Streekstra, G. J., Hardeman, M. R., Ince, C. and Grimbergen, C. A., Measurement of the Distribution of Red Blood Cell Deformability Using an Automated Rheoscope, *Cytometry*, Vol. 50, pp. 313-325, 2002.
7. Hénon, S., Lenormand, G., Richert, A. and Gallet, F., A New Determination of the Shear Modulus of the Human Erythrocyte Membrane Using Optical Tweezers, *Biophysical J.*, Vol. 76, pp. 1145-1151, 1999.
8. Mohandas, N. and Evans, E., Mechanical Properties of the Red Blood Cell Membrane in Relation to Molecular Structure and Genetic Defects, *Annual Reviews*, Vol. 23, pp. 787-818, 1994.
9. Korin, N., Bransky, A. and Dinnar, U., Theoretical Model and Experimental Study of Red Blood Cell (RBC) Deformation in Microchannels, *J. Biomechanics*, Vol. 40, pp. 2088-2095, 2007.
10. Katsumoto, Y., Hayashi, Y., Oshige, I., Omori, S., Kishii, N., Yasuda, A. and Asami, K., Dielectric sytometry with THree-dimensional Cellular Modelling, *Biophysical J.*, Vol. 95, pp. 3043-3047, 2008.
11. Goldsmith, H. L., Cokelet, G. R. and Gaehtgens, P., Robin Fåhraeus: Evolution of His Concepts in Cardiovascular Physiology, *American J. Physiological Society*, Vol. 257, pp. 1005-1015, 1989.
12. Olla, P., The Lift on a Tank-Treading Ellipsoidal Cell in a Shear Flow, *J. Physics 2 France*, Vol. 7, pp. 1533-1540, 1997.